Ductile failure prediction of thin notched aluminum plates subjected to combined tension-shear loading

A.R. Torabi [a], F. Berto [b], S.M.J. Razavi [b,*]

[a] *Fracture Research Laboratory, Faculty of New Sciences & Technologies, University of Tehran, P.O. Box 14395-1561, Tehran, Iran*

[b] *Department of Mechanical and Industrial Engineering, Norwegian University of Science and Technology (NTNU), Richard Birkelands vei 2b, 7491, Trondheim, Norway.*

Abstract

The main goal of the present research is to check the suitability of the combined Equivalent Material Concept-Averaged Strain Energy Density (ASED) failure criterion, called EMC-ASED, in predicting the load-carrying capacity (LCC) of notched aluminum plates subjected to mixed mode I/II loading. For this purpose, first, a set of experimental results on the LCC of thin V-notched rectangular Al 7075-T6 plates, that fail by large-scale yielding (LSY) regime, are taken from the open literature. Then, Al 7075-T6, which is a ductile material, is equated with an equivalent linear-elastic isotropic material by means of the EMC. Finally, the EMC is linked to the well-known ASED criterion to predict the LCC of the notched Al 7075-T6 plates. It is revealed that the experimental results could successfully be predicted by means of the combined EMC-ASED criterion without requiring complex and time-consuming elastic-plastic failure analyses.

[*] Corresponding author (S.M.J. Razavi): E-mail: javad.razavi@ntnu.no, Tel.: +47-930-24492

Keywords: Equivalent Material Concept (EMC); Averaged Strain Energy Density (ASED); Load-carrying capacity (LCC); V-notch; Aluminum plate; Ductile failure.

1. Introduction

Notches are extensively used in engineering components and structures, particularly in aero-structures. For instance, one can see wide O-shaped notches in the riveted joints, and U- and blunt V-notches in the access panels. Moreover, a large number of high-strength bolts and screws are normally used in aero-structures for joining two or more members in which the threads appear in blunt V-shape. Although notches are useful from the view point of engineering design, they are prone to the crack initiation as a result of the stress concentration at their neighborhood [1,2]. A notch threats the safety of structure which directly depends on the notch geometry and the material from which the structure is made. A higher level of the stress concentration results in a lower level of the structural safety. If the notched structural component is made of a brittle or quasi-brittle material, sudden fracture will be probable that may result in human and/or finance losses. Therefore, the lowest level of the design reliability is obtained when the structural component is weakened by a notch of great stress concentration and made of a brittle or quasi-brittle material [3-6]. Due to such a weak point of brittle materials (i.e. the sudden fracture), it is usually attempted in design of aero-structures to avoid employing brittle materials, unless otherwise essentially required, e.g. ceramics and graphite materials in high temperature applications etc.

Unlike brittle and quasi-brittle materials, ductile materials have widespread applications in engineering structures that their static failure is usually gradual and their final fracture takes

place in a stable manner [7,8]. Such a failure behavior is mainly due to significant plastic deformations [9,10]. If a notched component is made of a ductile material, it is expected that the crack initiation from the notch border and the crack growth will accompanied by a considerable plastic zone around the notch. The existence of such a significant plastic zone at the notch neighborhood and the slow growth of the likely crack emanating from the notch border increase the chance of detecting the crack before the final rupture and the notched member can be repaired or replaced [11,12]. Moreover, future similar failures can be prevented by means of re-designing the component etc.

A group of ductile materials with wide applications in aerospace structures are the aluminum alloys, particularly the series 2xxx and 7xxx. A review of the standard tensile stress-strain behavior of the aluminum alloys indicates that they exhibit negligible stain-hardening in the plastic zone such that their behavior in some branches of the mechanical engineering, e.g. the metal forming, is usually approximated by an ideal elastic-perfectly plastic behavior. The aluminum alloys Al 2024-Txxx and Al 7075-Txxx, where the index Txxx refers to the type of heat treatment, are extensively utilized in aero-structures and normally weakened by notches of various features, e.g. O-, U-, V-, blunt V- and key-hole notches. Considering that the safety of structure is vital in air vehicles, especially in manned vehicles like the civil airplanes etc., it is necessary to strictly evaluate the resistance of the aero-aluminum alloys against crack initiation from the notch border, so-called the notch fracture toughness (NFT), experimentally and/or theoretically [13-17]. A literature survey indicates that the number of researches on static failure of notched aluminum alloys is very limited and they have been mostly performed in recent years. Like the fracture researches on cracked bodies [18-20], the researches on notched members have also been started with the studies on pure mode I (i.e. the opening mode) loading conditions.

Two valuable research works have been recently published on static failure of notched aluminum specimens in which the tensile load-carrying capacity (LCC) of the specimens has been evaluated experimentally and theoretically. In the first work, static failure of the well-known compact-tension (CT) specimens weakened by U-notches of various tip radii and made of Al 7075-T651 has been experimentally investigated, and the mode I NFT has been measured [21]. To predict the experimentally obtained NFT values, the theory of critical distances (TCD) [22-25], which is a well-known brittle fracture theory, has been successfully employed [21]. In the second work, Vratnica et al. [26] have carried out several fracture experiments on the single-edge-notched-bend (SENB) specimens made of commercial aluminum alloy and weakened by U-notches of various tip radii under mode I loading conditions. They have experimentally measured the mode I NFT of the aluminum alloy and successfully predicted the corresponding experimental values by means of a fracture criterion. While both Madrazo et al., [21] and Vratnica et al. [26] have reported good agreement between the experimental and theoretical results, using only the linear-elastic stress distributions around the notch in the theoretical predictions and disregarding the effects of the plastic region at the notch neighborhood on static strength of the aluminum specimens could be questionable. Such a disregard could be justified by Madrazo et al., because of the relatively large thickness of the specimens, while in ref. [21] the specimen thickness has not been large enough, providing considerable plastic deformations around the notch at the onset of crack initiation from the notch tip.

Recently, Torabi and co-researchers [27-29] have published three papers in which ductile failure of notched aluminum plates under pure mode I loading conditions has been investigated experimentally and theoretically. In Torabi et al., [27] the tensile load-carrying capacity (LCC) of thin rectangular plates made of Al 7075-T6 and weakened by blunt V-notches has been

experimentally measured and the corresponding LCCs have been successfully predicted by using the Equivalent Material Concept (EMC) in conjunction with two stress-based brittle fracture criteria in the context of the linear elastic notch fracture mechanics (LENFM), namely the point-stress (PS) and mean-stress (MS) criteria. It has been reported that the V-notched Al 7075-T6 plates fail by the moderate-scale yielding (MSY) regime. A similar work has also been performed by Torabi et al., [28] on the same V-notched specimen, but made of Al 6061-T6 which has been much more ductile than Al 7075-T6. It has been found that the combination of the EMC with the two brittle fracture criteria is also successful in predicting the LCCs of the Al 6061-T6 specimens. The other important finding in ref. [28] has been that the Al 6061-T6 specimens fail by the large-scale yielding (LSY) regime. By taking into account the results of previous two last given references simultaneously, it can be concluded that the EMC could well be combined with the stress-based brittle fracture criteria for predicting the LCC of V-notched aluminum members regardless of the amount of plastic deformations around the notch at failure. With the aim to study the effects of notch feature (i.e. the notch stress gradient) on suitability of such a combination, Torabi et al. [29] have performed similar assessments on U-notched Al 7075-T6 and Al 6061-T6 plates subjected to tensile loading. The specimen as the same with that studied by Torabi et al. [27,28] containing a U-notch has been employed to conduct ductile fracture tests on Al 7075-T6 and Al 6061-T6. It has been found that like V-notched specimens, the U-notched Al 7075-T6 and Al 6061-T6 specimens fail by the MSY and LSY regimes, respectively. Moreover, the suitability of the combination of the EMC with the two stress-based criteria in predicting the LCC of the U-notched aluminum specimens has been revealed, regardless of the type of the failure regime [29]. Other criteria are available and valid for cracked components but not for the notched components.

Under mixed mode I/II loading conditions, however, the same specimen but with inclined V- and U-shaped notches has been studied in Torabi et al. [6,30,31] for ductile failure. From the experimental point of view, the main difference between the mode I and mixed mode I/II results has been that the entire V- and U-notched aluminum specimens fail by the LSY regime under mixed mode loading, probably because of the significant contribution of shear deformations in forming the plastic zone around the notch at failure. In the theoretical predictions of the LCC, it has been revealed that the EMC could well be combined with the maximum tangential stress (MTS) and mean-stress (MS) brittle fracture criteria [6,30,31].

The literature review reveals that a paper has been published on ductile failure of aluminum alloys containing notches under pure mode II loading [32]. Ghahremaninezhad et al. [32] studied experimentally the crack nucleation from the border of a V-notch in Al 6061-T6 under pure in-plane shear loading. The well-known Arcan specimen configuration was utilized to produce pure mode II loading conditions around the V-notch. The experiments were simulated by means of the Johnson–Cook model and its modified version and it was found that it is essential to account for great levels of the local strain prior to the crack initiation for capturing the large plastic deformations observed in the fracture tests. Some valuable microscopic studied were also performed using the scanning electron microscope (SEM) in order to determine the sites of crack nucleation etc. [32].

In the present research, it is tried to check the suitability of the EMC-ASED criterion also for mixed mode I/II loading conditions under which the failure regime tends from the MSY to LSY due to significant plastic zone around the notch at failure as a result of large shear deformations. For this purpose, the EMC-ASED criterion is described and formulated in forthcoming sections and the experimentally obtained LCCs reported in ref. [33] are predicted. A very good agreement

is shown to exist between the experimental results and the theoretical predictions, demonstrating that the suitability of the EMC-ASED criterion is independent of the ductile failure regime and the mode of in-plane loading.

2. Fracture test results on notched aluminum plates reported in the literature

A set of mixed mode I/II ductile fracture test results have been recently published by Torabi et al. [33] on thin Al 7075-T6 plates weakened by blunt V-shaped notches. The chemical composition and the mechanical properties of the tested material are presented in Tables 1 and 2, respectively. Moreover, the standard tensile engineering and true stress-strain curves of the material are represented in Fig. 1, from which it is evident that the tested Al 7075-T6 is a ductile material and shows negligible strain-hardening in the plastic zone [33]

Table 1. Chemical composition of the tested Al 7075-T6 [33].

Table 2. Mechanical properties of the tested Al 7075-T6 [33].

Fig. 1. Standard tensile engineering and true stress-strain curves of Al 7075-T6 [33].

In Torabi et al., [33] a rectangular plate of 2 mm thick weakened by a central rhombic slit with four blunt V-shaped corners has been considered for conducting the mixed mode I/II fracture

experiments. Fig. 2 schematically shows the specimen including the loading and geometric parameters. As seen in Fig. 2, the loading mode, e.g. pure mode I and mixed mode I/II, on the two main blunt V-notches can be controlled by the notch rotation angle β, which is the angle between the abscissa and the notch bisector line. When $\beta = 0$, the bisector line lies on the abscissa and the two blunt V-notches are subjected to pure mode I loading. As β enhances from zero, the contribution of mode II loading increases and the mode of loading on V-notches changes from pure mode I towards mixed mode I/II. It is evident that various values of β result in different values of mode mixity.

Fig. 2. The V-notched specimen subjected to mixed mode I/II loading [33].

As seen in Fig. 2, the parameters 2α, ρ, 2a, L, W, β, and P denote the notch angle, the notch radius, twice the notch length (i.e. the slot length), the specimen length, the specimen width, the notch rotation angle, and the remotely applied tensile load, respectively. The values of these parameters considered in the experiments are as follows: $2\alpha = 30^o$, 60^o, and 90^o; $\rho = 1$, 2, and 4 mm; 2a = 25 mm; L = 160 mm; W = 50 mm. Also, the values of β for the notch angles of 30^o, 60^o, and 90^o have been considered to be equal to (0^o, 30^o and 60^o), (0^o and 30^o) and (0^o and 30^o), respectively. Thickness of the entire specimens has been constant and equal to 2 mm. By repeating each test three times, sixty-three fracture experiments have been totally carried out [33].

Table 3 summarizes the experimental values of the load-carrying capacity (LCC) of the V-notched Al 7075-T6 thin plates reported by Torabi et al., [33] for different notch angles and radii. Note that in Table 3, the parameters P_i (i=1, 2, 3) and P_{av} denote the LCC in the three repeated tests and the average of the three LCCs, respectively.

Table 3. The experimentally recorded LCCs of the V-notched Al 7075-T6 specimens for different notch angles and radii [33]

Some of the broken V-notched Al 7075-T6 plates are shown in Fig. 3. As can be seen in Fig. 3b, the ligament experiences large plastic deformations which are clear with naked eye. Such plastic deformations suggest the existence of large-scale yielding (LSY) failure regime. Moreover, the inclined fracture surface shown in Fig. 3c proves that the type of failure in the tested V-notched Al 7075-T6 plates is the ductile rupture, not brittle fracture. Besides, it has been reported in ref. [33] that the experimental observations and the numerical simulations confirm that the crack initiation from the V-notch round border takes place by the LSY regime. Hence, the fracture criteria in the context of the LENFM are not fundamentally permitted to be used for failure predictions. In forthcoming sections, in order to avoid time-consuming and complex elastic-plastic failure analyses, a permit is first taken by means of the Equivalent Material Concept (EMC) to utilize the LENFM-based brittle fracture criteria for ductile failure prediction of the Al 7075-T6 plates. Then, the EMC is linked to the Average Strain Energy Density (ASED) brittle fracture criterion for predicting the LCCs of the V-notched Al 7075-T6 thin plates failed by the LSY regime under mixed mode I/II loading.

Fig. 3. Some of the broken V-notched Al 7075-T6 plates.

3. The Equivalent Material Concept

The Equivalent Material Concept (EMC), originally proposed by Torabi et al. [34] is a concept by which it is possible to equate a ductile material exhibiting elastic-plastic behavior and having valid *K*-based fracture toughness (i.e. K_{Ic} or K_c) with a virtual brittle material having the linear elastic behavior till final fracture. The main reason for such an equality is to avoid using the failure criteria in the context of the elastic-plastic fracture mechanics (EPFM) like the critical J-integral, the crack tip opening displacement (CTOD), and the crack tip opening angle (CTOA) etc. [35] because of their complexity and time consumption.

The sole unequal material property between the real ductile and virtual brittle materials is the ultimate tensile strength. It is assumed in the EMC that both the materials absorb the same amount of tensile strain energy density (SED) for the crack initiation to happen. Actually, the ductile material absorbs the SED mainly by its considerable strain to failure (the crack initiation or the necking is assumed to be the failure mode) while the equivalent material by its high strength. Trivially, it is expected that the ultimate tensile strength of the equivalent material becomes greater than that of the real ductile material. If tensile strength of the equivalent material is known, it can be utilized together with the fracture toughness K_{Ic} or K_c in various fracture criteria in the context of the linear elastic notch fracture mechanics (LENFM) for predicting the crack initiation from the notch border in ductile members without performing elastic-plastic failure analyses. It has been reported in Torabi et al., [33] that the maximum load that the V-notched Al 7075-T6 specimens could sustain is obtained at the onset of crack

initiation from the notch border. Therefore, it is possible to predict the load-carrying capacity (LCC) of the specimens by means of the EMC (together with the LENFM-based criteria).

Assuming a power-law relationship between the stress and the plastic strain for the ductile material, the tensile strength of the equivalent material has been reported in Torabi et al., [30] as

$$\sigma_f^* = \sqrt{{\sigma_Y}^2 + \frac{2EK}{n+1}\left[{\varepsilon_{u,true}}^{n+1} - (0.002)^{n+1}\right]} \quad (1)$$

where the parameters σ_f^*, σ_Y, E, K, n, and $\varepsilon_{u,\text{true}}$ denote the tensile strength of the equivalent material, yield strength of the ductile material, elastic modulus, strain-hardening coefficient, strain-hardening exponent, and the true plastic strain at the ultimate point, respectively. Eq. (2) can simply be used to calculate the value of $\varepsilon_{u,\text{true}}$, in which ε_u is the engineering plastic strain at the ultimate point.

$$\varepsilon_{u,true} = \ln(1+\varepsilon_u) \quad (2)$$

The values of the parameters K_{Ic} (or K_c) and σ_f^* can now be utilized in different LENFM-based fracture criteria for LCC prediction of notched ductile components that fail by considerable plastic zone around the notch. For the tested Al 7075-T6, the value of σ_f^* is calculated by means of the material properties provided in Table 2 and using Eq. (1) to be equal to 1845 MPa.

In forthcoming sections, first, the well-known averaged strain energy density (ASED) fracture criterion is briefly described and linked to the EMC. Then, the experimental LCCs of the V-notched Al 7075-T6 thin plates provided in Table 3 are theoretically predicted by means of the EMC-ASED criterion.

4. A brief description of the Averaged Strain Energy Density criterion

The most critical point for designers is surely to select an appropriate failure model to assess the load-carrying capacity of notched components. With this aim, a strain energy density based criterion has been first proposed by Lazzarin and co-authors [36,37].

The averaged strain energy density (ASED) approach as formulated by Lazzarin et al. [36], suggests that brittle fracture occurs when the SED averaged over material dependent control volume reaches a critical value W_c which depends on the material. This value is independent of the notch geometry. Under linear elastic hypotheses the material dependent characteristic volume is depends on the ultimate tensile strength and on the fracture toughness K_{Ic}. The approach was first proposed for sharp V-notches under tensile loading and in-plane mixed mode loadings. Later on it has been applied also to blunt notches and a wide review is reported in Berto et al., [37]. Some recent contribution on averaged SED can be also found in Gallo et al. [38-42].

Dealing with sharp cracks, the volume is simply a circle of radius R_c centered at the crack tip (Fig. 4b). Under plane-strain hypotheses, the critical radius R_c, can be estimated by using the expression reported below [43]:

$$R_c = \frac{(1+\nu)(5-8\nu)}{4\pi}\left(\frac{K_{Ic}}{\sigma_u}\right)^2 \tag{3}$$

Fig. 4. Control volume (area) for sharp V-notch (a), sharp crack (b) and blunt V-notch (c) under mode I loading. Distance $r_0 = \rho \times (\pi - 2\alpha)/(2\pi - 2\alpha)$.

Fig. 5. Control volume (area) under in-plane mixed mode loading.

In Eq. (3), K_{Ic} is mode I the fracture toughness, ν the Poisson's ratio and σ_u the ultimate tensile strength of material.

Dealing with a sharp V-notch, the control volume assumes a circular shape of radius R_c centered at the notch tip (Fig. 4a) while for a V-notch with a finite radius under mode I loading, the volume becomes a crescent shape shown in Fig. 4c, where R_c is the depth measured along the notch bisector line. The external radius of the crescent shape volume is equal to R_c+r_0. Parameter r_0 is the distance between the notch tip and the origin of the local coordinate system (see Fig. 4c). Such a distance depends on the V-notch opening angle 2α, according to the expression $r_0 = \rho\,(\pi-2\alpha)/(2\pi-2\alpha)$.

The concept of equivalent local mode I, although not exact in principle, has been successfully used to deal with mixed mode problems [37]. In particular the ASED was generalized from pure tension loading to mixed mode loading considering the hypothesis of an equivalent local mode I along the normal line to the notch edge, at the point where the principal stress reaches its maximum value (see Fig. 5). The approach was employed to assess the brittle failure of U-notched samples made of PMMA and tested at -60°C under mixed mode loading [44]. According to the coordinate system shown in Fig. 5, the stress component $\sigma_{\theta\theta}$ normalized to its maximum value occurring along the notch edge has been found equal to the mode I theoretical solution reported by Lazzarin et al. [45]. This observation leads to the conclusion that under mixed mode loading the line normal to the notch edge and starting from the point of maximum principal stress behaves as a virtual bisector line under pure mode I, confirming the applicability of the equivalent local mode I concept (see Fig. 6).

Fig. 6. Comparison between theoretical mode I stress distribution and FE results along the normal from the point of maximum principal stress; $2\alpha=60°$. The results are referred to the higher values of angle β corresponding to prevalent mode II.

5. Application of EMC in combination with ASED criterion

The averaged strain energy density approach is applied here considering the material properties of the equivalent material. The critical strain energy density, $W_{c,EMC}$, is evaluated by using the following equations and considering σ_f^* = 1845 MPa:

$$W_{c,EMC} = \frac{\sigma_f^{*2}}{2E} \tag{4}$$

The critical strain energy density results to be equal to 23.97 MJ/m^3. The control radius R_c is evaluated by using Eq. (3) with $\sigma_u = \sigma_f^*$ = 1845 MPa. It is found R_c = 0.183 mm. The ASED occurring inside the control volume embracing the edges of V-notches ($\overline{W}$) is calculated numerically by using the FE code ANSYS. For each notch geometry, a FE model is created by accurately defining the control volume, where the strain energy density should be averaged. According to the procedure described in the previous section, the control volume is centered at the point of maximum principal stress along the curvilinear edge of the notch. All FE analyses are performed by using eight-node 2D finite elements (PLANE 183) under plane-strain conditions. A detail of the mesh, of the principal stress contour lines and of the SED contour lines are depicted in Fig. 7a, 7b and 7c, respectively.

Fig. 7: Mesh used in the FE model (a) maximum principal stress (b) and iso-strain energy density contour lines (c) for the case ρ=1, 2α=30° and β=60°.

5. Results and discussion

Table 4 summarizes the results of the experimental, numerical and theoretical analyses for V-notched specimens considered in the present investigation. Three different notch radii (ρ = 1, 2, 4 mm) are analyzed by means of the ASED approach with different inclination of the notch. In particular, Table 4 reports the experimental loads to failure (*P*) for all notch radii ρ, notch inclination β and notch opening angle 2α compared with the theoretical values (P_{ASED}) based on the ASED evaluation. P_{ASED} is the theoretical load obtained by keeping constant the critical strain energy density, $W_{c,EMC}$, equal to 23.97 MJ/m^3.

Table 4. Critical loads predicted by means of ASED criterion in combination with EMC.

In the last columns of the table, the relative deviations between the values of the experimental failure loads and the theoretical results obtained by means of ASED criterion are reported to show the accuracy of the employed approach. Δ is defined as the ratio between the experimental load and the theoretical one for each case.

It is well visible from Table 4 that the majority of the assessed results are well inside the scatter band ranging between ± 20% with many of the results falling inside the scatter ranging between ± 10%. A sound synthesis expressed in terms of the square root of the local strain energy normalized with respect to the critical energy of the material, $W_{c,EMC}$, as a function of the notch opening angle is depicted in Fig. 8. The parameter plotted in the figure is proportional to the failure load. The main aim of the figure is to show that the averaged SED is able to take into account not only the influence of the notch geometry but also of the mode mixity on the final fracture assessment. Also from the graphical point of view, it is obvious that the great majority of values fall inside a scatter ranging from 0.80 to 1.20 with some data inside a scatter ranging from 0.90 to 1.10. The synthesis confirms also the choice of the control volume which seems to be suitable to characterize the material behavior under mixed mode I/II loading. The scatter of the experimental data presented here is in very good agreement with the recent database in terms of ASED reported in a recent review of the approach and dealing with brittle and quasi-brittle failure [46].

Fig. 8. Synthesis of fracture data in terms of normalized ASED.

A number of researchers investigated the 3D stress state in different geometries of notched components considering constraint factors and stress concentration factors throughout the specimen thickness [47]. The main features of the in-plane stress distributions and the variability of the stress concentration factor as a function of the plate thickness were investigated in numerous researches [48-50]. The same methodology can be considered for the notched

components made of ductile materials in order to evaluate the effect of specimen thickness on the accuracy of the predicted failure loads by EMC-ASED criterion.

6. Conclusions

This manuscript is aimed to analyze the in-plane mixed mode fracture behavior of Al 7075-T6 thin plates weakened by V-notches with different bluntness. Some fracture tests were carried out on rectangular plates containing central blunt V-shaped notches. The experimental observations indicated large plastic deformations around the notch tip at the crack initiation, demonstrating large-scale yielding (LSY) failure regime for the aluminum plates. The loads corresponding to the onset of crack initiation from the notch tip were recorded. To theoretically predict the experimental results, the Equivalent Material Concept was employed together with the Averaged Strain Energy Density over a material-dependent control volume. Without requiring time-consuming and complex elastic-plastic finite element analyses, it was shown that the combination of the Averaged Strain Energy Density approach and the Equivalent Material Concept can successfully predict the load-carrying capacity of the V-notched Al 7075-T6 plates characterized by large plastic deformations ahead of the notch tip.

References

[1] Z. He, A. Kotousov, F. Berto, Effect of vertex singularities on stress intensities near plate free surfaces, Fatigue Fract. Eng. Mater. Struct. 38 (2015) 860-869.

[2] P. Lazzarin, M. Zappalorto, F. Berto, Three-dimensional stress fields due to notches in plates

under linear elastic and elastic–plastic conditions, Fatigue Fract. Eng. Mater. Struct. 38(2) (2015) 140-153.

[3] A.R. Torabi, M. Fakoor, M.A. Darbani, Pure shear fracture study in a brittle graphite material containing a U-notch, Int. J. Damage Mech. 23 (2014) 839-854.

[4] A.R. Torabi, F. Berto, Strain energy density to assess mode II fracture in U-notched disk-type graphite plates, Int. J. Damage Mech. 23 (2014) 917-930.

[5] J.X. Liu, T. El Sayed, A quasi-static algorithm that includes effects of characteristic time scales for simulating failures in brittle materials, Int. J. Damage Mech. 23 (2014) 83-103.

[6] A.R. Torabi, S.H. Amininejad, Brittle fracture in V-notches with end holes, Int. J. Damage Mech. 24 (2015) 529-545.

[7] H.S. Liu, M.W. Fu, Prediction and analysis of ductile fracture in sheet metal forming—Part II: Application of the modified Ayada criterion, Int. J. Damage Mech. 25(2) (2016) 120-140.

[8] V. Pensée, L. Morin, D. Kondo, A damage model for ductile porous materials with a spherically anisotropic matrix, Int. J. Damage Mech. 25(3) (2016) 315-335.

[9] K. Ali, D. Peng, R. Jones, R.R.K. Singh, X.L. Zhao, A.J. McMillan, F. Berto, Crack growth in a naturally corroded bridge steel, Fatigue Fract. Eng. Mater. Struct. (in press). DOI: 10.1111/ffe.12568

[10] S.V. Panin, P.O. Maruschak, I.V. Vlasov, D.D. Moiseenko, F. Berto, R.T. Bishchak, A. Vinogradov, The role of notch tip shape and radius on deformation mechanisms of 12Cr1MoV steel under impact loading. Part 1. Energy parameters of fracture, Fatigue Fract.

Eng. Mater. Struct. (in press). DOI: 10.1111/ffe.12533

[11] F. Berto, A. Campagnolo, P. Lazzarin, Fatigue strength of severely notched specimens made of Ti–6Al–4V under multiaxial loading, Fatigue Fract. Eng. Mater. Struct. 38(5) (2015) 503-517.

[12] O. Fergani, F. Berto, T. Welo, S.Y. Liang, Analytical modelling of residual stress in additive manufacturing, Fatigue Fract. Eng. Mater. Struct. (in press). DOI: 10.1111/ffe.12560

[13] S.M.J. Razavi, M.R. Ayatollahi, C. Sommitsch, C. Moser, Retardation of fatigue crack growth in high strength steel S690 using a modified stop-hole technique, Eng. Fract. Mech. 169 (2017) 226–237.

[14] M.R. Ayatollahi, S.M.J. Razavi, C. Sommitsch, C. Moser, Fatigue life extension by crack repair using double stop-hole technique, Mater. Sci. Forum 879 (2017) 3-8.

[15] M. R. Ayatollahi, S.M.J. Razavi, M.Y. Yahya, Mixed mode fatigue crack initiation and growth in a CT specimen repaired by stop hole technique, Eng. Fract. Mech. 145 (2015) 115-127.

[16] M.R. Ayatollahi, S.M.J. Razavi, H.R. Chamani, A numerical study on the effect of symmetric crack flank holes on fatigue life extension of a SENT specimen, Fatigue Fract. Eng. Mater. Struct. 37(10) (2014) 1153-1164.

[17] M.R. Ayatollahi, S.M.J. Razavi, H.R. Chamani, Fatigue Life Extension by Crack Repair Using Stop-hole Technique under Pure Mode-I and Pure mode-II Loading Conditions,

Procedia Eng. 74 (2014) 18–21.

[18] P. Gallo, T. Sumigawa, T. Kitamura, F. Berto, Evaluation of the strain energy density control volume for a nanoscale singular stress field, Fatigue Fract. Eng. Mater. Struct. 39(12) (2016) 1557-1564.

[19] A. Campagnolo, G. Meneghetti, F. Berto, Rapid finite element evaluation of the averaged strain energy density of mixed-mode (I+ II) crack tip fields including the T-stress contribution, Fatigue Fract. Eng. Mater. Struct. 39(8) (2016) 982-998.

[20] L.P. Pook, A. Campagnolo, F. Berto, Coupled fracture modes of discs and plates under anti-plane loading and a disc under in-plane shear loading, Fatigue Fract. Eng. Mater. Struct. 39 (2016) 924–938.

[21] V. Madrazo, S. Cicero, I.A. Carrascal, On the Point Method and the Line Method notch effect predictions in Al7075-T651, Eng. Fract. Mech. 79 (2012) 363–379.

[22] L. Susmel, D. Taylor, On the use of the Theory of Critical Distances to predict static failures in ductile metallic materials containing different geometrical features, Eng. Fract. Mech. 75 (2008) 4410–4421.

[23] D. Taylor, The Theory of Critical Distances Applied to the Prediction of Brittle Fracture in Metallic Materials, SID Structural Integrity Durability 1 (2005) 145–154.

[24] D. Taylor, Predicting the fracture strength of ceramic materials using the theory of critical distances, Eng. Fract. Mech. 71 (2008) 2407–2416.

[25] S. Kasiri, D. Taylor, A critical distance study of stress concentrations in bone, J. Biomech. 41 (2008) 603–609.

[26] M. Vratnica, G. Pluvinage, P. Jodin, Z. Cvijović, M. Rakin, Z. Burzić, K. Gerić, Notch fracture toughness of high-strength Al alloys, Mater. Design 44 (2013) 303–310.

[27] A. Torabi, M. Alaei, Application of the equivalent material concept to ductile failure prediction of blunt V-notches encountering moderate-scale yielding, Int. J. Damage Mech. (in Press) DOI: 10.1177/1056789515625451

[28] A. Torabi, M. Keshavarzian, Tensile crack initiation from a blunt V-notch border in ductile plates in the presence of large plasticity at the notch vicinity, Int. J. Terrasp. Sci. Eng. 8 (2016) 93–101.

[29] A. Torabi, R. Habibi, B. Mohammad Hosseini, On the Ability of the Equivalent Material Concept in Predicting Ductile Failure of U-Notches under Moderate- and Large-Scale Yielding Conditions, Phys. Mesomech. 18 (2015) 337–347.

[30] A. Torabi, M. Keshavarzian, Evaluation of the load-carrying capacity of notched ductile plates under mixed mode loading, Theor. Appl. Fract. Mech. 85(B) (2016) 375–386.

[31] A. Torabi, F. Berto, A. Campagnolo, Elastic-plastic fracture analysis of notched Al 7075-T6 plates by means of the local energy combined with the equivalent material concept, Phys. Mesomech. 19 (2016) 204–214.

[32] A. Ghahremaninezhad, K. Ravi-Chandar, Crack nucleation from a notch in a ductile material under shear dominant loading, Int. J. Fract. 184 (2013) 253-266.

[33] A. Torabi, M. Alaei, Mixed-mode ductile failure analysis of V-notched Al 7075-T6 thin sheets Engineering, Fract. Mech. 150 (2015) 70–95.

[34] A. Torabi, Estimation of tensile load-bearing capacity of ductile metallic materials

weakened by a V-notch: The equivalent material concept, Mater. Sci. Eng. A 536 (2012) 249–255.

[35] A. Saxena, Nonlinear fracture mechanics for engineers, CRC Press LLC, Florida, 1998.

[36] P. Lazzarin, R. Zambardi, A finite-volume-energy based approach to predict the static and fatigue behavior of components with sharp V-shaped notches, Int. J. Fract. 112 (2001) 275–298.

[37] F. Berto, P. Lazzarin, A review of the volume-based strain energy density approach applied to V-notches and welded structures, Theor. Appl. Fract. Mech. 52 (2009) 183–194.

[38] P. Gallo, F. Berto, Advanced Materials for Applications at High Temperature: Fatigue Assessment by Means of Local Strain Energy Density, Adv. Eng. Mater. (in Press) DOI:10.1002/adem.201500547

[39] P. Gallo, F. Berto, High temperature fatigue tests and crack growth in 40CrMoV13.9 notched components, Frattura ed Integrita Strutturale 9 (2015) 180-189.

[40] P. Gallo, F. Berto, G. Glinka, Analysis of creep stresses and strains around sharp and blunt V-notches, Theor. Appl. Fract. Mech. (in Press) DOI: 10.1016/j.tafmec.2016.06.003

[41] P. Gallo, T. Sumigawa, T. Kitamura, F. Berto, Analysis of creep stresses and strains around sharp and blunt V-notches, Fatigue Fract. Eng. Mater. Struct. (in Press) DOI: 10.1111/ffe.12468.

[42] P. Gallo, F. Berto, G. Glinka, Generalized approach to estimation of strains and stresses at blunt V-notches under non-localized creep, Fatigue Fract. Eng. Mater. Struct. 39(3) (2016) 292-306.

[43] Z. Yosibash, A. Bussiba, I. Gilad, Failure criteria for brittle elastic materials, Int. J. Fract. 125(3) (2004) 307–333.

[44] F.J. Gómez, M. Elices, F. Berto, P. Lazzarin, Local strain energy to assess the static failure of U-notches in plates under mixed mode loading, J. Fract. 145 (2007) 29–45.

[45] P. Lazzarin, S. Filippi, A generalized stress intensity factor to be applied to rounded V-shaped notches, Int. J. Solids Struct. 43 (2006) 2461–2478.

[46] F. Berto, P. Lazzarin, Recent developments in brittle and quasi-brittle failure assessment of engineering materials by means of local approaches, Mater. Sci. Eng. Reports 75 (2014) 1–48.

[47] A. Kotousov, P. Lazzarin, F. Berto, L.P. Pook, Three-dimensional stress states at crack tip induced by shear and anti-plane loading, Eng. Fract. Mech. 108 (2013) 65-74.

[48] F. Berto, A. Kotousov, P. Lazzarin, L.P. Pook, On scale effect in plates weakened by rounded V-notches and subjected to in-plane shear loading, Int. J . Fract. 180 (2013) 111-118.

[49] L.P. Pook, A. Campagnolo, F. Berto, P. Lazzarin, Coupled fracture mode of a cracked plate under anti-plane loading, Eng. Fract. Mech. 134 (2015) 391-403.

[50] F. Berto, P. Lazzarin, A. Kotousov, L.P. Pook, Induced out-of-plane mode at the tip of blunt lateral notches and holes under in-plane shear loading, Fatigue Fract. Eng. Mater. Struct. 35 (2012) 538-555.

Figure Captions

Fig. 1. Standard tensile engineering and true stress-strain curves of Al 7075-T6 [10].

Fig. 2. The V-notched specimen subjected to mixed mode I/II loading [10].

Fig. 3. Some of the broken V-notched Al 7075-T6 plates.

Fig. 4. Control volume (area) for sharp V-notch (a), sharp crack (b) and blunt V-notch (c) under mode I loading. Distance $r_0 = \rho \times (\pi - 2\alpha)/(2\pi - 2\alpha)$.

Fig. 5. Control volume (area) under in-plane mixed mode loading.

Fig. 6. Comparison between theoretical mode I stress distribution and FE results along the normal from the point of maximum principal stress; $2\alpha=60°$. The results are referred to the higher values of angle β corresponding to prevalent mode II.

Fig. 7: Mesh used in the FE model (a) maximum principal stress (b) and iso-strain energy density contour lines (c) for the case $\rho=1$, $2\alpha=30°$ and $\beta=60°$.

Fig. 8. Synthesis of fracture data in terms of normalized ASED.

Table Captions

Table 1. Chemical composition of the tested Al 7075-T6 [10].

Table 2. Mechanical properties of the tested Al 7075-T6 [10].

Table 3. The experimentally recorded LCCs of the V-notched Al 7075-T6 specimens for different notch angles and radii [10].

Table 4. Critical loads predicted by means of ASED criterion in combination with EMC.

Table 1. Chemical composition of the tested Al 7075-T6 [10].

Element	Si	Fe	Cu	Mn	Mg	Zn	Ni	Cr	Pb	Sn	Ti
Weight (%)	0.06	0.32	1.72	0.03	2.44	4.63	0.004	0.2	0.002	0.001	0.037
Element	B	Cd	Bi	Ca	P	Sb	V	Zr	Co	Li	Al
Weight (%)	0.001	0.001	0	0.001	0.001	0.001	0.007	0.017	0.003	0.001	90.5

Table 2. Mechanical properties of the tested Al 7075-T6 [10].

Material Property	Value
Elastic modulus, E (GPa)	71
Poisson's ratio	0.33
Tensile yield strength (MPa)	521
Ultimate tensile strength (MPa)	583
Elongation at break (%)	5.8
Engineering strain at maximum load	0.047
True fracture stress (MPa)	610
Fracture toughness, K_c (MPa.$\sqrt{m}$)	50
Strain-hardening coefficient, (MPa)	698
Strain-hardening exponent	0.046

Table 3. The experimentally recorded LCCs of the V-notched Al 7075-T6 specimens for different notch angles and radii [10].

2α (deg.)	ρ (mm)	β (deg.)	P_1 (N)	P_2 (N)	P_3 (N)	$P_{av.}$ (N)
30	1	0	27554	27337	27870	27587
30	2	0	27826	28271	28146	28081
30	4	0	28290	28661	28529	28493
60	1	0	27550	27918	27874	27781
60	2	0	27922	28496	27546	27988
60	4	0	27874	28304	28702	28293
90	1	0	26012	23776	25328	25039
90	2	0	28337	27616	26358	27437
90	4	0	27900	28098	28113	28037
30	1	30	30912	30375	31556	30948
30	2	30	30486	31280	31376	31047
30	4	30	30500	30828	30622	30650
30	1	60	39344	39285	39753	39461
30	2	60	39767	39377	39149	39431
30	4	60	37851	37325	37166	37447
60	1	30	30798	30780	29478	30352
60	2	30	31269	31152	28922	30448
60	4	30	29548	30809	31015	30457
90	1	30	30549	29581	30916	30349
90	2	30	30846	30258	31104	30736
90	4	30	30074	30265	29158	29832

Table 4. Critical load predicted by means of ASED criterion in combination with EMC.

β	ρ (mm)	2α (deg)	P_1 (N)	P_2 (N)	P_3 (N)	P_{EMC} (N)	Δ_1	Δ_2	Δ_3
0	1	30	27554	27337	27870	23653	1.16	1.16	1.18
0	2	30	27826	28271	28146	28496	0.98	0.99	0.99
0	4	30	28290	28661	28529	35019	0.81	0.82	0.81
0	1	60	27550	27918	27874	22534	1.22	1.24	1.24
0	2	60	27922	28496	27547	27411	1.02	1.04	1.00
0	4	60	27874	28304	28702	33929	0.82	0.83	0.85
0	1	90	26012	23776	25328	21565	1.21	1.10	1.17
0	2	90	28337	27616	26358	26073	1.09	1.06	1.01
0	4	90	27900	28098	28113	32283	0.86	0.87	0.87
30	1	30	30913	30375	31556	26402	1.17	1.15	1.20
30	2	30	30486	31280	31376	31884	0.96	0.98	0.98
30	4	30	30501	30828	30622	37665	0.81	0.82	0.81
30	1	60	30799	30780	29478	26559	1.16	1.16	1.11
30	2	60	31269	31152	28922	31302	1.00	1.00	0.92
30	4	60	29548	30810	31016	37572	0.79	0.82	0.83
30	1	90	30549	29581	30916	29998	1.02	0.99	1.03
30	2	90	30846	30258	31104	34556	0.89	0.88	0.90
30	4	90	30074	30265	29158	39949	0.75	0.76	0.73
60	1	30	39344	39285	39753	41584	0.95	0.94	0.96
60	2	30	39767	39377	39149	45416	0.88	0.87	0.86
60	4	30	37851	37325	37166	50717	0.75	0.74	0.73

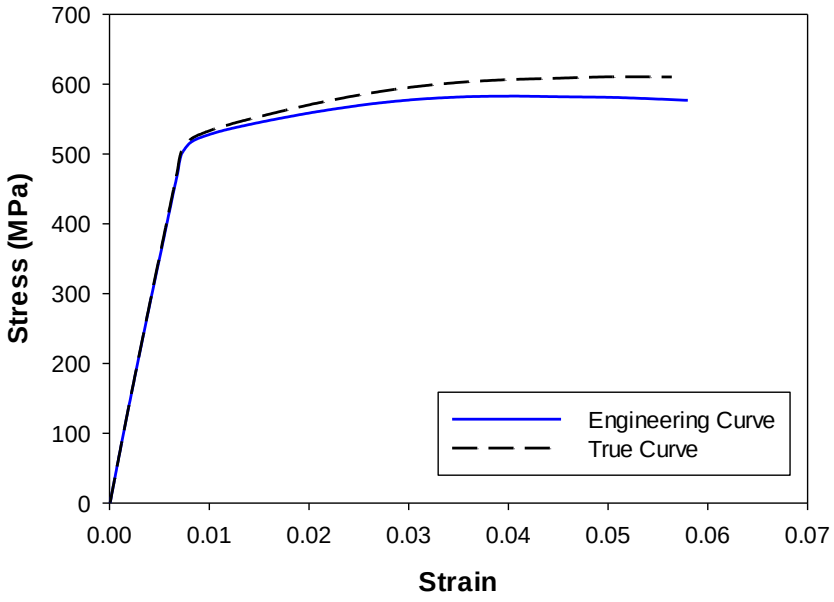

Fig. 1. Standard tensile engineering and true stress-strain curves of Al 7075-T6 [10].

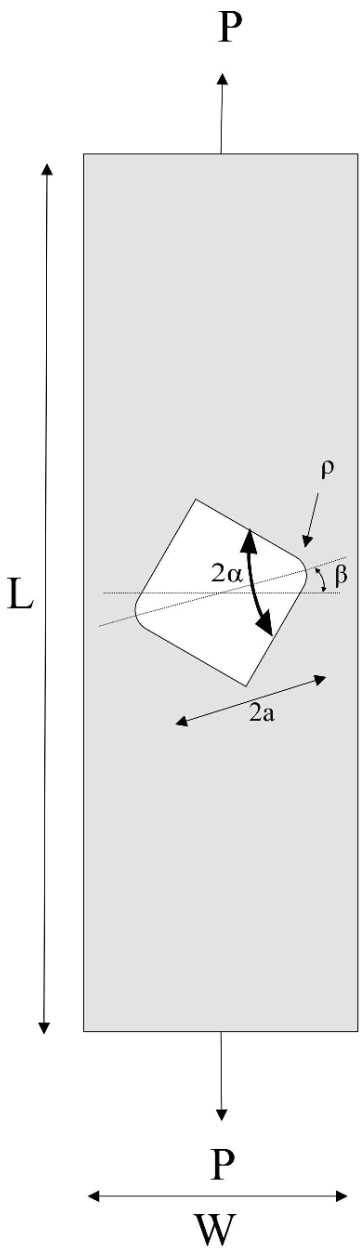

Fig. 2. The V-notched specimen subjected to mixed mode I/II loading [10].

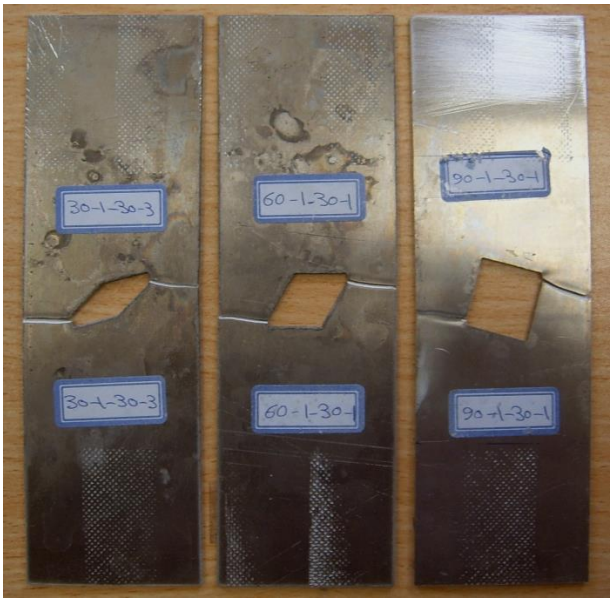

(a) A full view of the broken plates

(b) Large plastic deformations at the ligament

(c) Inclined fracture surface

Fig. 3. Some of the broken V-notched Al 7075-T6 plates.

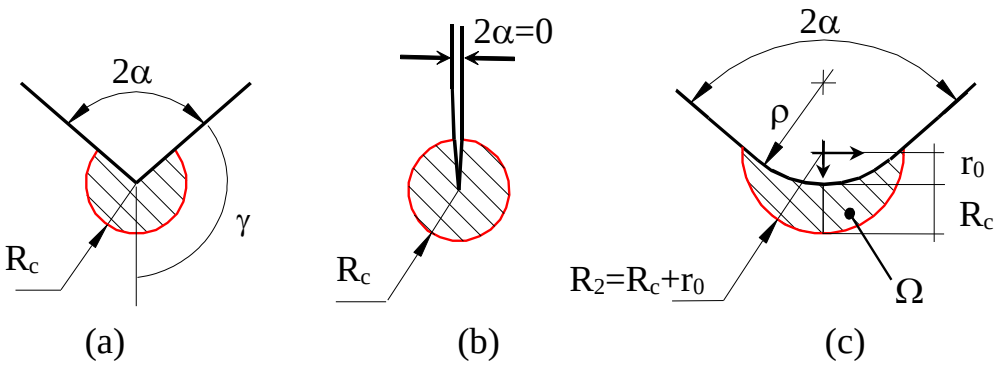

Fig. 4. Control volume (area) for sharp V-notch (a), sharp crack (b) and blunt V-notch (c) under mode I loading. Distance $r_0 = \rho \times (\pi - 2\alpha)/(2\pi - 2\alpha)$

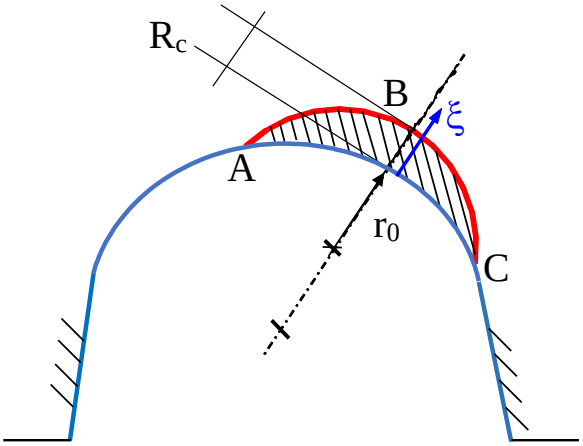

Fig. 5. Control volume (area) under in-plane mixed mode loading.

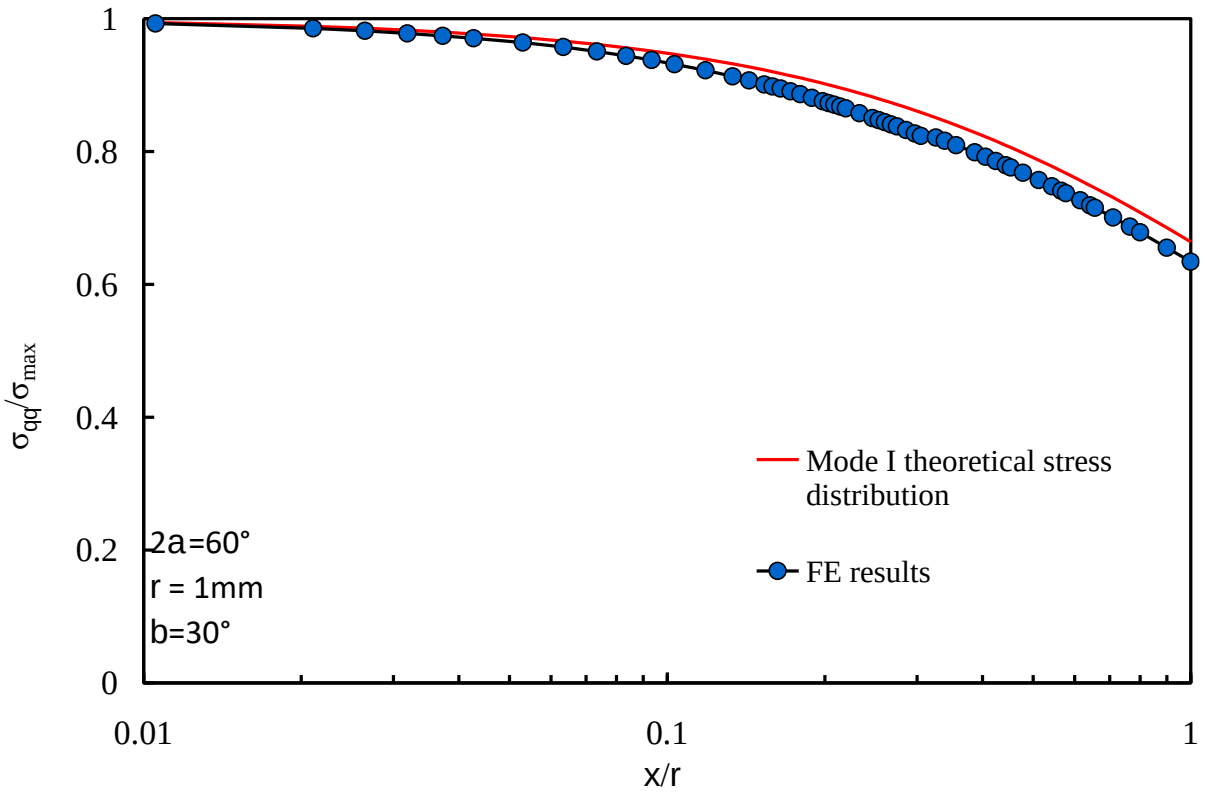

Fig. 6. Comparison between theoretical mode I stress distribution and FE results along the normal from the point of maximum principal stress; $2\alpha=60°$. The results are referred to the higher values of angle β corresponding to prevalent mode II.

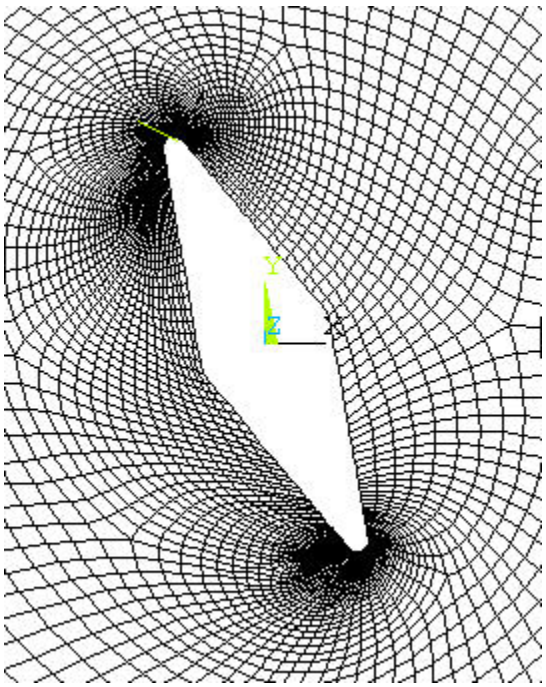
Y
Z
X

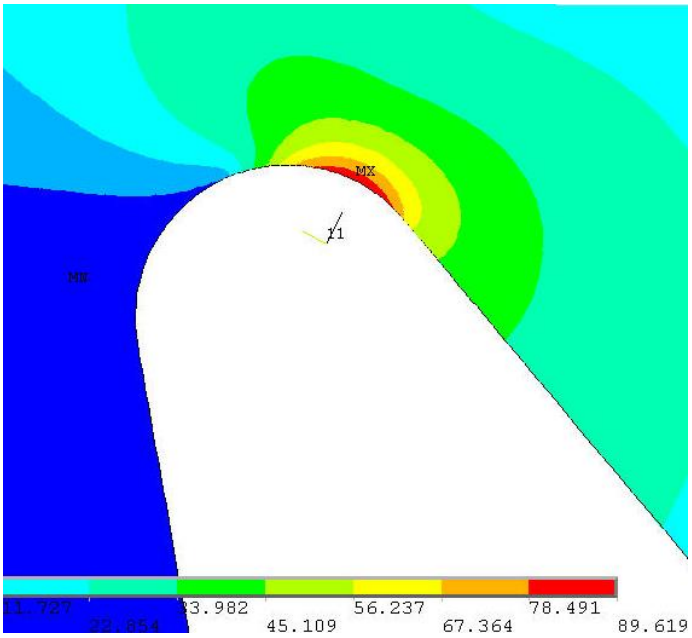
MX
MN
1
11.727
22.854
33.982
45.109
56.237
67.364
78.491
89.619

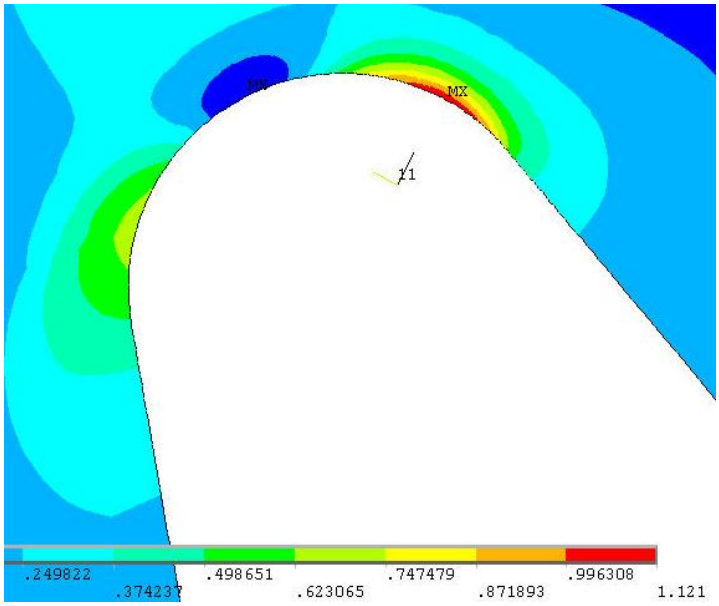

Fig. 7: Mesh used in the FE model (a) maximum principal stress (b) and iso-strain energy density contour lines (c) for the case $\rho=1$, $2\alpha=30°$ and $\beta=60°$.

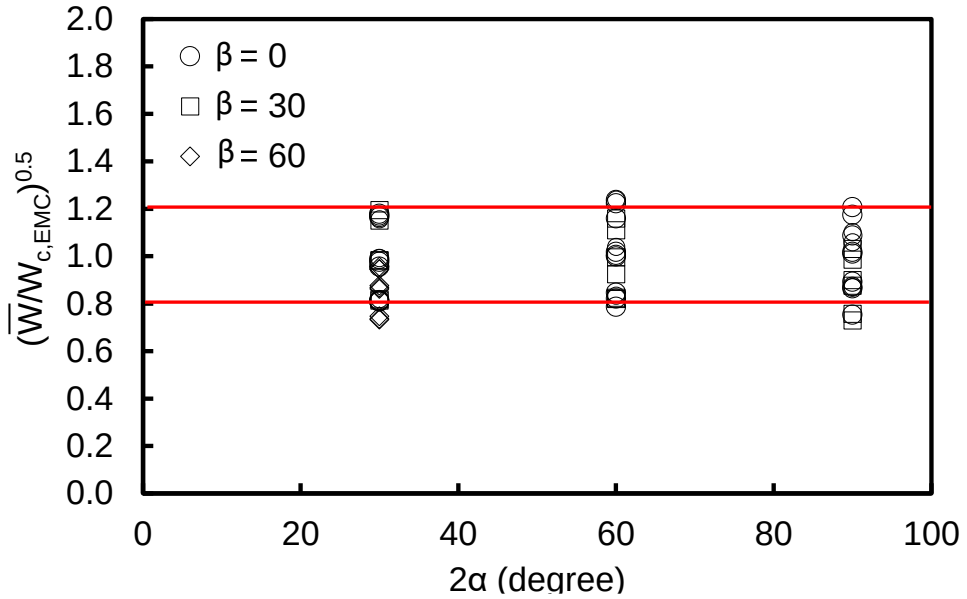

Fig. 8. Synthesis of fracture data in terms of normalized ASED.